Physics of Fluids

RESEARCH ARTICLE | APRIL 05 2023

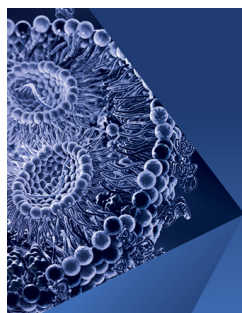# Investigation of Ultraviolet-C light-emitting diode for airborne disinfection in air duct FREE

Special Collection: Flow and the Virus , Flow and the Virus

Li Hongying (李红英) ✉ ⓘD ; Shan Xuechuan (单学传); Ba Te (巴特); Liu Yu Chan (刘玉婵);
Kang Chang-Wei (江功伟) ⓘD ; Hing Candice Au Ka (區嘉馨); Nitin Loganathan; Uvarajan M. Velayutham ⓘD

Check for updates

View Online   Export Citation

17 August 2024 08:19:13

Physics of Fluids

Special Topic:

Flow and Lipid Nanoparticles

Guest Editors: Richard Braatz and Mona Kanso

Submit Today!

AIP Publishing

Investigation of Ultraviolet-C light-emitting diode for airborne disinfection in air duct

Hongying Li (李红英),[1,a] Xuechuan Shan (单学传),[2] Te Ba (巴特),[1] Yu Chan Liu (刘玉婵),[2] Chang-Wei Kang (江功伟),[1] Candice Au Ka Hing (區嘉馨),[2] Nitin Loganathan,[3] and Uvarajan M. Velayutham[4]

AFFILIATIONS

[1]Institute of High Performance Computing (IHPC), Agency for Science, Technology and Research (A∗STAR), 1 Fusionopolis Way, #16-16 Connexis, Singapore 138632, Republic of Singapore
[2]Singapore Institute of Manufacturing Technology (SIMTech), Agency for Science, Technology and Research (A∗STAR), 2 Fusionopolis Way, Singapore 138634, Republic of Singapore
[3]YSQ International Pte Ltd 401 Commonwealth Dr., #07-01, Singapore 149598, Republic of Singapore
[4]Ember Technologies Pte Ltd, 20A Tanjong Pagar Road, Singapore 088443, Republic of Singapore

Note: This paper is part of the special topic, Flow and the Virus.
a)Author to whom correspondence should be addressed: lih@ihpc.a-star.edu.sg

ABSTRACT

Given the current coronavirus (COVID-19) situation around the world, we may have to face a long-term battle with coronavirus. It is necessary to prepare and stay resilient with some other techniques to improve air quality in buildings, especially in clinics and hospitals. In this paper, we have developed Ultraviolet-C (UVC) light-emitting diode (LED) modules which can be implemented in air ducts in heating, ventilation, and air conditioning system for airborne disinfection. An LED module is designed with LED panels as the basic unit so that it is easy to scale up to accommodate for air ducts with different sizes. Both experiments and simulations are carried out to study its disinfection performance. The results show that more than 76% and 85% of the pathogen can be inactivated within 60 and 90 min, respectively, in a meeting room with a volume of 107 m^3 by using one LED module. Simulations for two LED modules show that the disinfection efficacy is more than two times compared to that of one LED module. In addition to the pathogen used in the experiments, the disinfection performance of the LED module for inactivation of SARS-CoV-2 virus based on the literature is investigated numerically. It shows that more than 99.70% of pathogens receive UV dose larger than 4.47 J/m^2, leading to an almost 89.10% disinfection rate for SARS-CoV-2 virus within one hour using the two LED modules in the same meeting room.

Published under an exclusive license by AIP Publishing. https://doi.org/10.1063/5.0144729

NOMENCLATURE

a	Absorption coefficient (1/m)
c_1,c_2,c_3	Constant
$C_D, C_{1\varepsilon}, C_{2\varepsilon}$	Constant
D	UV dose (J/m^2)
d_p	Particle diameter (m)
F	Force (N)
$G\kappa$	Production of turbulent energy (kg/m s^3)
$\vec{g}$	Gravity vector (m/s^2)
I	Fluence rate (W/m^2)
I	Radiation intensity (W/m^2)
l	Characteristic of reactor (m)
n	Refractive index
P	Pressure (Pa)
Re	Reynolds number
$\vec{s}$	Direction vector (m/s)
T	Temperature (°C)
t	Time (s)
$\vec{u}$	Velocity vector (m/s)
x,y,z	Cartesian coordinate

Greek symbols

ε	Energy dissipation rate (m^2/s^3)
k	Kinetic energy (m^2/s^2)
μ	Dynamic viscosity (kg/m s)
ρ	Density (kg/m^3)
σ	Stefan Boltzmann constant (W/m^2 K^4)
$\sigma_\kappa, \sigma_\varepsilon$	Empirical constant

Subscripts

p	Particles
t	Turbulent flow

I. INTRODUCTION

The ongoing pandemic of coronavirus disease (COVID-19) has caused a large global crisis with a death toll in millions.[1] A reason for its infectiousness lies in the facts of spreading, which in the case of COVID-19, in the form of droplet transmission through the air route.[2] Airborne transmission of COVID-19 has been widely recognized as one of the main transmission routes. It was supported by much epidemiological evidence during the pandemic.[3–6] Such airborne persists in air due to a low settling rate[7] and poses threats to healthy people who are in the same room as the infected person. Mitigation measures related to the airborne transmission are challenging. Thus, the experience of the ongoing COVID-19 pandemic and the possible future pandemics requires the implementation for the new control systems to improve indoor air quality.

Indoor air quality can be improved by introducing fresh outdoor air into the indoor environment. However, this is not feasible for most of the systems due to the extensive energy consumption to cool/heat the fresh air to the indoor conditions. Some other methods such as air filters,[8] air purifier,[9] and ionizers[10] are adopted as additional measures in many indoor places to mitigate COVID-19 transmission. The U.S. Environmental Protection Agency (EPA) has released new guidance on the best practices to improve indoor air quality (IAQ) for combating COVID-19.[11] Generally, the practical recommendations such as optimization of outdoor fresh air intake and the use of filtration in the Heating, Ventilation, and Air Conditioning (HVAC) systems are proposed in the report. Of interest is the suggestion for the usage of Ultraviolet Germicidal Irradiation (UVGI) system for disinfection air in buildings.

UVGI is a well-established method for air disinfection to prevent the spread of infectious diseases. The history of UVGI for air disinfection can be traced back to 19th century.[12] Since the outbreak of COVID-19, extensive research has demonstrated that Ultraviolet-C (UVC) irradiation is highly effective in inactivation of SARS-CoV-2.[13–17] UVC can pass through the cell wall of the microorganisms and absorbed by the protein and nucleotides so that it can disrupt the structure of DNA or RNA of the microorganism. This inactivates microorganisms for functioning and reproducing itself. Upper-room UVGI and In-duct UVGI are two primary applications for UVGI air disinfection. Upper-room UVGI is to irradiate UV energy to the space which is above occupants' head. This usually requires a qualified HVAC professional to ensure the system is installed properly. Special precautions are needed as UV energy directed or reflected into the occupied space has the potential to cause temporary eye or skin damage. Therefore, such technique is still not well developed. Compared with upper-room UVGI, in-duct UVGI avoids directly irradiating UV energy to the occupants. It is designed to disinfect air as it passes through the HVAC system and usually installed in the air ducts with enclosed space. In addition to the air disinfection, in-duct UVGI can also be used to disinfect surfaces inside HVAC systems. Therefore, it has been highly recommended for air disinfection in hospitals.[18,19] However, the design and optimization of in-duct UVGI systems are poorly understood due to the limited knowledge for UVC Light-emitting diode (LED) performance, such as LED output characteristics, the microbial UV dose response, and energy consumption.[20]

Of central importance to the efficacy of in-duct UVGI for air disinfection is the device which generates UV radiation. Generally, two main types of UV lamps, i.e., mercury-based UV lamps and UVC LED light, are commonly used. Currently, mercury-based UV lamps are popularly adopted as disinfection products given its high-power output and low cost. However, mercury-based UV lamps are usually served with big device and fixtures. They are larger and heavier compared with UVC LED lights. UVC generation of ozone is also one of another great concerns for mercury-based UV lamps. As COVID-19 pandemic continues, there has been growing demand for disinfection device using UVC LED. The most prominent advantage of UVC LED compared with mercury-based UV lamps is its miniaturization in size. Although there are still many unsolved issues such as the degradation of UVC LED and the decreased performance of UVC LED due to the decrease of the optical power, its improved efficacy and robustness in recent years made it a more promising approach in air disinfection.[21]

UVC LED for air disinfection has been studied extensively.[22–26] Kim and Kang[22] have adopted UVC LED to inactivate viral, bacteria, and fungal aerosols in chamber-type air disinfection system. They found that UVC LED can effectively inactivate micro-organism regardless of taxonomic classification. Mathebula et al.[23] used UVC LED assemble to disinfect airborne *Mycobacterium tuberculosis*. They concluded that UVC LED can be used to replace mercury-based UV lamps for air disinfection. A novel upper room rotating UVC LED irradiation system for disinfection of indoor bioaerosols was proposed by Nunayon et al.[24] Their test results demonstrated that UVC LED system can inactivate and decrease the concentration of bioaerosols significantly. Lai and Nunayon[25] designed a compact UVC LED system to disinfect pathogens generated by toilet flushing. Their results demonstrated that LEDs were effective in inactivating three different microbes, i.e., *E. coli*, *S. typhimurium*, and *S. epidermidis* which are commonly found in toilet environment. Nunayon et al.[26] studied air disinfection in ventilation duct flow with the combined effect of UVC and ion polarities. The results indicated that such a method could be a potential way to minimize the transmission risk in indoor environments. Despite all the efforts mentioned above, the study of UVC LED for air disinfection in air duct is still at its early stage. Limited work can be found for the design of UVC LED and its performance of airborne disinfection for the usage in the HVAC system. The current study will try to fill this gap.

In this work, we designed UVC LED modules with LED panels as a basic unit for air disinfection. The modules can be scaled up and installed in the air duct in HVAC systems. The premium advantage of the proposed design is its flexibilities which are easily modified to tailor for different HVAC systems. Multiple UVC LED modules can be used to achieve high disinfection rate according to the environmental requirements. The numerical model is developed for the disinfection performance study of the designs. The simulation work is performed based on the commercial software ANSYS FLUENT[27] with user-defined functions to calculate the UV dose absorbed by a pathogen. The developed numerical model is then applied to study COVID-19 disinfection by using the UVC LED module. It is hoped that the current work can shed light on the usage of UVC LED to mitigate COVID-19 aerosol transmission in indoors.
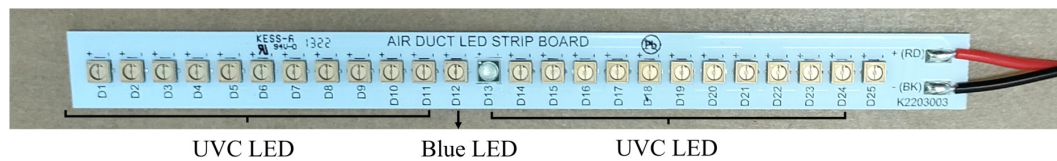
FIG. 1. PCB board with one LED strip.

II. EXPERIMENTS

A. LED chips and LED strips

The LED strip with 24 UVC LED and one blue LED used in the current work is shown in Fig. 1. The 24 UVC LEDs (D1-D12, D14-D24) can emit UVC photons in the range of 270–280 nm which is proven to be effective to inactivate SARS-CoV-2 virus.[13–17] The blue LED (D13) in the middle of the strip is used to indicate the working status of the system to ensure safety. The UVC LED chips are purchased from TaoYuan Electron (HK) Limited. Each UVC LED chip is 3.5×3.5 mm, and the radiation power is in the range of 5–8 mW. The LED strip is mounted on one printed circuit board (PCB). The dimensions of PCB are 140 mm in length and 12 mm in width. On the PCB, every four UVC LEDs are connected in parallel to form a group. Each group of UVC LED is connected in series with other groups. An LED driver is used to provide a constant current driving mode to PCB LED strip. The driving current is up to 500 mA. With this design arrangement, the PCB circuit and LED strip is compact and easy to assemble.

B. LED panels and LED modules

It is well known that more than 70% of the energy consumed by LED is converted into heat.[28] Therefore, thermal management is critical to ensure UVC LED works at its best performance with a long lifespan. We proposed a design which combines heat pipes and fins as heat sinks to dissipate the heat generated by the LEDs. The cross section of the rectangular heat pipe used in our design is 12 mm (width) $\times$ 4 mm (height) $\times$ 500 mm (length). Figure 2 illustrates one heat pipe on which PCB with one LED strip are attached. Thermal conductive double-sided tape was used to adhere the PCB board onto the heat pipe. The number of LED strips can be adjusted based on different applications. For example, two LED strips can be attached on one PCB and pasted to one side of the heat pipe in series. Conversely of the heat pipe, we can also attach another PCB with two LED strips to increase the UVC irradiation intensity.

For the ease of scaling up by adopting more LED strips in the air duct, an LED panel is designed as a basic unit. The LED panel consists of one or multiple heat pipes and fins. The LED strips are pasted to the heat pipes while the heat pipes are mounted to the fins. Multiple heat pipes can be aligned side by side to form a more powerful LED panel with high UVC intensity. As shown in Fig. 3(a), there are three heat pipes in one LED panel. Two such panels can be placed face to face to improve both the UV intensity (UVI) and its uniformity in the air duct. The fins of the heat sinks can either be installed at the back or in front of LED strips, as seen from Figs. 3(a) and 3(b), respectively.
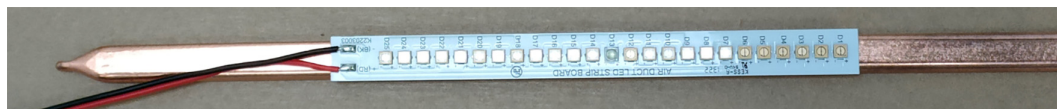

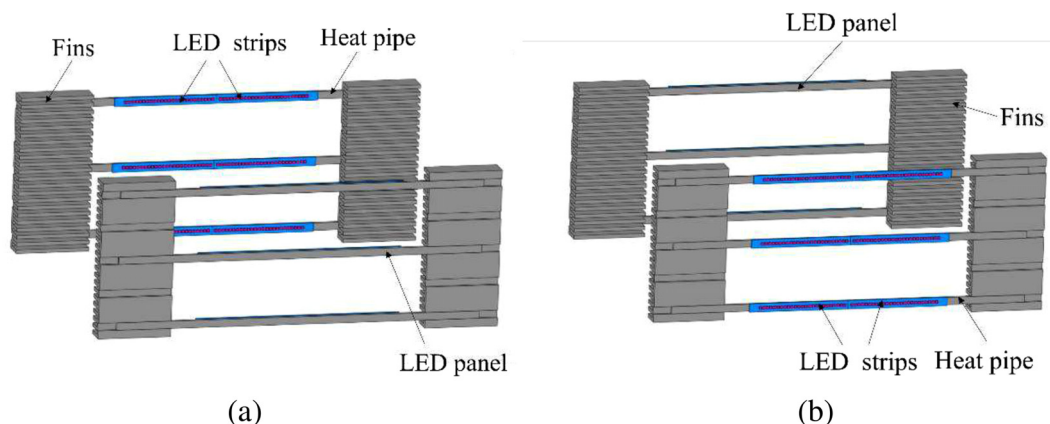**FIG. 2.** Heat pipe with one LED strip attached on it.

(a)   (b)

FIG. 3. Fins of the heat sink located (a) in front and (b) at back of LED strips.
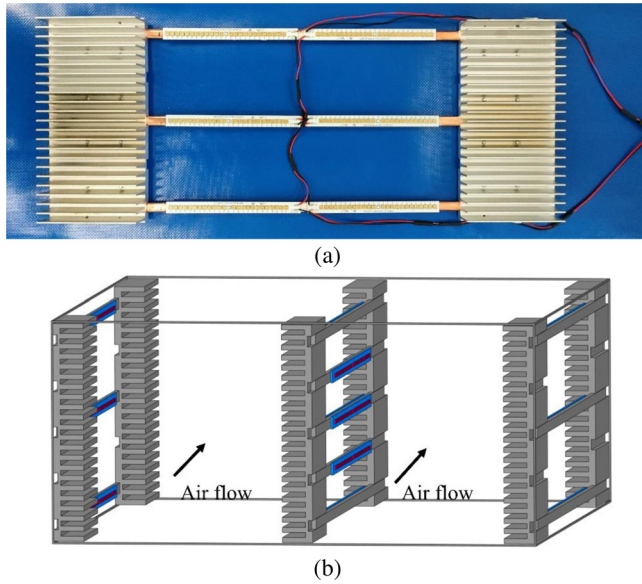
FIG. 4. (a) An LED panel with three heat pipes and six LED strips and (b) schematic diagram of one LED module with three LED panels.

Figure 4(a) shows one LED panel that consists of three heat pipes. Two LED strips are attached on one heat pipe. The ends of each heat pipe are attached to fin-shaped heat sinks. The LED panels are supported by frames shown in Fig. 4(b), and it is called an LED module. The LED module can be aligned in parallel to the flow direction. When the LED module is slotted into the air duct, the gap between the LED module and the duct wall can be minimized, leading to minimized non-disinfected air volume. As shown in Fig. 4(b), the LED panels at two sides near the duct wall have three heat pipes each. The central LED panel has six heat pipes, among which three heat pipes face to the left and the other three heat pipes face to the right. The width and height of the frame is changeable to suit various size of air duct. Furthermore, several LED modules can be aligned along air flow direction in series or stacked along the duct height direction for scaling up to fit large sized air ducts.

C. Air duct

Figure 5(a) shows the prototype of air duct we designed and fabricated to mimic air flow in an actual air duct. The dimensions of the rectangular air duct are $500 \times 250 \times 1200$ mm for the width, height, and length, respectively. A fan is connected to the rectangular air duct through a soft pipe. The rotation speed of the fan can be adjusted through AC voltage so that the flow rate inside of the duct can be controled. Figure 5(b) shows the mesh we used for part of the air duct in our simulation which will be discussed in Sec. III. In this air duct, the total number of LEDs used is 576. They are divided into 24 strips, and these 24 strips are arranged in three LED panels, respectively. In each of the strip, there are 48 LEDs which are aligned in parallel to the flow direction. The middle LED pannel has both LED strips facing to the left and right directions of the channel, respectively.
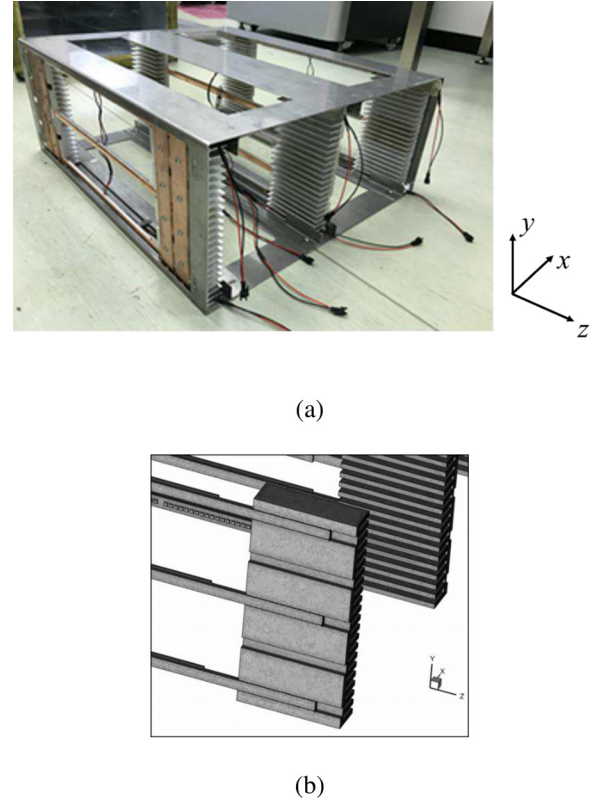

FIG. 5. (a) LED panels and (b) mesh distribution for part of the LED panel.

III. NUMERICAL SIMULATION

A. Mathematical model

The problem considered in the experiments involves fluid flow, radiation heat transfer, and pathogen transport. The flow is assumed to be incompressible. Steady-state flow is considered in the current work. The Buoyancy effect is not included in the model as air temperature increase in the system is not significant. This will be discussed in Sec. IV A. The mathematical equations governing the transport of mass, momentum with considering turbulent flow, are given by

$$\nabla \cdot (\rho \vec{u}) = 0, \tag{1}$$

$$\nabla \cdot (\rho \vec{u} \vec{u}) = -\nabla P + \nabla \cdot \left[(\mu + \mu_t)(\nabla \vec{u} + \nabla \vec{u}^T) \right] - \nabla \cdot \left(\frac{2}{3} \rho k \vec{I} \right), \tag{2}$$

where $\vec{u}$ is the velocity vector, ρ is the density of air, P is the pressure, μ is the viscosity of air, k is the turbulent kinetic energy, and μ_t is the eddy viscosity. For the case considering turbulent flow, the k-ε model[29] is adopted as it has been well validated by researchers for simulation of fluid flow in different applications with the comparison against their experimental results.[30–32] The equations for solving k and ε are

$$\nabla \cdot (\rho \vec{u} k) = \nabla \cdot \left(\frac{\mu_t}{\sigma_k} \nabla k \right) + G_k - \rho \varepsilon, \tag{3}$$

$$\nabla \cdot (\rho \vec{u} \varepsilon) = \nabla \cdot \left(\frac{\mu_t}{\sigma_\varepsilon} \nabla \varepsilon \right) + \frac{\varepsilon}{k} (C_{1\varepsilon} G_k - C_{2\varepsilon} \rho \varepsilon), \qquad (4)$$

where $C_{1\varepsilon}$ and $C_{2\varepsilon}$ are the constants with values of 1.44 and 1.92, respectively. σ_κ and σ_ε are 1.00 and 1.3, respectively.[33] These values of constants have been obtained by numerous iterations of data fitting for a wide range of turbulent flows.[34] G_k is the production of turbulence kinetic energy. The eddy viscosity μ_t is given by

$$\mu_t = \rho C_\mu \frac{\kappa^2}{\varepsilon}, \qquad (5)$$

where C_μ equals to 0.09.

The radiative transfer equation based on the discrete ordinates model[35] is written as

$$\nabla \cdot (I \cdot \vec{s}) + aI = an^2 \frac{\sigma T^4}{\pi}, \qquad (6)$$

where a is the absorption coefficient, n is the refractive index, σ is the Stefan–Boltzmann constant, I is the UV intensity, T is the temperature, and $\vec{s}$ is the direction vector. Through the order of magnitude analysis, the term on the right-hand side of Eq. (6) is two orders smaller than the other terms on the left-hand side. Therefore, a low temperature of 1 K is patched to the fluid for radiation simulation to minimize the effect of thermal radiation from temperature differences between the fluid and the lamp sleeves.

A constant mass flow rate is used for the inlet boundary, and an atmosphere pressure boundary condition is used at the outlet boundary. The walls are assumed to be no-slip. For the radiation transport equation, a constant radiation flux boundary condition is used for all the lamp walls. The rest walls including the reactor wall and baffle walls are assumed to be opaque.

The initial values for k and ε are[34]

$$k = \frac{2}{3} (uJ)^2, \qquad (7)$$

where

$$J = 0.16 Re^{-1/8}, \qquad (8)$$

$$\varepsilon = C_\mu^{0.75} \frac{\kappa^{1.5}}{l}, \qquad (9)$$

where l is the characteristic length that is chosen to be the diameter of the reactor in this study.

The pathogen is treated as solid particles. The trajectory of the pathogen was predicted through the integration of the force on the particles based on the Lagrangian reference frame.[36] The mathematical formulation for particle movement is[37]

$$\frac{d\vec{u}_p}{dt} = F_D (\vec{u}_p - \vec{u}) + \frac{\vec{g}(\rho_p - \rho)}{\rho_p} + \vec{F}. \qquad (10)$$

The subscript p represents the pathogen. u_p and u are the pathogen and air velocity, respectively. F_D is the drag force exerted on air by the pathogen.[27] $\vec{F}$ is the other forces involved such as virtual force and pressure gradient force. The mathematical expression of F_D is

$$F_D = \frac{18\mu}{\rho_p d_p^2} + \frac{C_D Re}{24}, \qquad (11)$$

where C_D is the drag force coefficient and Re is the Reynolds number, d_p is the pathogen particle diameter. The expressions for C_D[37] and Re are, respectively,

$$C_D = c_1 + \frac{c_2}{Re} + \frac{c_3}{Re^2}, \qquad (12)$$

$$Re = \frac{\rho d_p |\vec{u}_p - \vec{u}|}{\mu}, \qquad (13)$$

where c_1, c_2, and c_3 are constants, and they are valid for spherical particles for all ranges of Re. These constants are expressed as follows:

$$c_1, c_2, c_3 = \begin{cases} 0, 24, 0, & 0 < Re < 0.1, \\ 3.69, 22.73, 0.0903, & 0.1 < Re < 1, \\ 1.222, 29.1667, -3.8889, & 1 < Re < 10, \\ 0.6167, 46.5, -116.67, & 10 < Re < 100, \\ 0.3644, 98.33, -2778, & 100 < Re < 1000, \\ 0.357, 148.62, -47\,500, & 1000 < Re < 5000, \\ 0.46, -490.546, 578\,700, & 5000 < Re < 10\,000, \\ 0.5191, -1662.5, 5\,416\,700, & Re \geq 10\,000. \end{cases}$$
$$(14)$$

The virtual force and the force induced by the pressure gradient are considered with the mathematical formulation of[37]

$$\vec{F} = 0.5 \frac{\rho}{\rho_p} \frac{d(\vec{u} - \vec{u}_p)}{dt} + \frac{\rho}{\rho_p} \vec{u}_p \nabla \cdot \vec{u}_p. \qquad (15)$$

The particles are injected through the inlet boundary with the injection files with a random distribution profile. These particles flow out of the reactor through the outlet boundary. The walls are set to be reflected with no energy loss occurring when particles collided with walls. The initial velocity of the micro-organism particles is set to be 0. One-way coupling is used as the volume fraction of the micro-organism particles is quite small.

B. Numerical procedure

The procedure for the simulation of the current problem is divided into three steps based on the models used for solving different problems. These are (1) simulation of air flow in air duct, (2) simulation of UV irradiation in the air duct, and (3) pathogen trajectory simulation in air duct. These three components are modeled sequentially in the simulation. All the simulation work is performed based on ANSYS FLUENT platform[27] with user-defined function implemented to calculate UV dose absorbed by the pathogen along its trajectory. The UV dose absorbed by the pathogen is calculated by

$$D = \int_0^t I \, dt, \qquad (16)$$

where I is the UV intensity. The time step size used in the simulation for particle trajectory is 10^{-5}.

The mesh is generated based on ANSYS Workbench platform. 30 million cells are used for one LED module with 576 chips. There are 5–7 meshes along the fin thickness direction. Three different

pathogen numbers, i.e., 5000, 10 000, and 20 000 are compared for particle sensitivity study. It is found that the differences for the average UV dose between 5000 and 10 000 pathogens, 10 000 and 20 000 pathogens, are 5.2% and 1.3%, respectively. Therefore, 10 000 pathogens are adopted in the case studies. Additional cases for different inlet distributions of the pathogen including uniform and Rosin–Rammler distribution profiles under the same total number of pathogens are performed. The results show that the average UV dose among random, uniform, and Rosin–Rammler distributions is within 5%. Therefore, a random distribution of the particles is used at the inlet boundary.

C. Validation

The numerical model was validated against experimental data for ballast water treatment systems.[38,39] Further validation is performed for air disinfection in the biosafety cabinet (BSC) chamber as shown in Fig. 6(a). We installed a 275 nm UVC LED prototype at the bottom of the chamber. Pathogen is injected from the left by the nebulizer (Omron NE-C801). The fan inside the prototype sucks air and pathogen to flow through the UVC LED prototype where the pathogen absorbs UV light. The flow rate in the chamber is 125 l/min measured by a rotameter. In this test, *E. coli* is used as the pathogen. *E. coli* (ATCC25922) strain was obtained from American Type Culture Collection and stored at $-20\,^\circ$C. To prepare the experimental culture stock, $5\,\mu$l of the original *E. coli* (ATCC25922) stock was added to 50 ml of LB-broth (Miller) and placed in an incubator shaker overnight at $37\,^\circ$C and 150 rpm. The bacterial stock was grown until it

reached an OD of 0.5–0.6 at OD 600. The culture was then serially diluted to obtain a concentration of 107 CFU/ml. 1 ml of the 107 CFU/ml of *E. coli* was mixed with 2 ml of LB broth to obtain the working stock concentration of 107 CFU/3 ml. Bacterial inactivation was measured by culturing them onto agar plates. Following exposure to the UVC radiation, the aerosols were collected on tryptic soy agar plates. They are directly transferred into an incubator and left overnight at a temperature of $37\,^\circ$C. The number of CFU was then counted manually and compared with the zero-dose control to assess the disinfection efficiency of the BSC chamber.

The dimensions of the UVC LED prototype are 613 mm (length) $\times$ 216 mm (width) $\times$ 48 mm (height), respectively. There are four rows of UVC LED installed at the top wall of the channel along the flow direction seen from Fig. 6(b). Fins are arranged at the external wall of the prototype to dissipate heat generated by the LED strips inside of the chamber. Each row has 24 discrete LED chips with a total number of 96 chips in four strips. The power for each chip is 7 mW. Two scenarios are performed in the experiments, i.e., without and with activation of the UVC LED in the prototype, respectively. The scenarios without activation of UVC LED will be served as a benchmark case to evaluate the efficacy of the UVC LED prototype. Simulations are carried out with similar scenarios as the experiments. In both experiments and simulations, a total number of 30 K *E. coli* are injected into the BSC chamber. The diameters of the *E. coli* range from 1 to 8 μm with a random size distribution. The average diameter for all the *E. coli* is 4.49 μm. Figure 7 shows the survival rate of *E. coli* under different times between the experiments and simulations. It is also clear to see that almost all the injected *E. coli* is killed or inactivated within 10 min when the UVC LED module operates. However, only 50% of the injected *E. coli* is settled to the floor within the same period with UVC LED off. This shows that UVC LED is very effective to disinfect air. Special attention needs to be paid for the case with UVC LED off. In the first 5 min, most of the pathogens are suspended in air due to their small sizes. This will potentially pose aerosol transmission risk. In general, good agreement is achieved between experiments and simulations. It demonstrates the capability of the developed
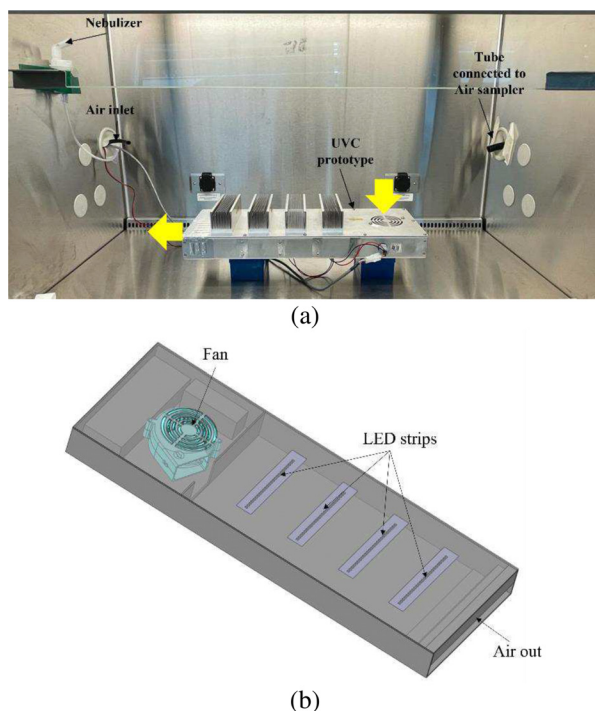

(a)

(b)

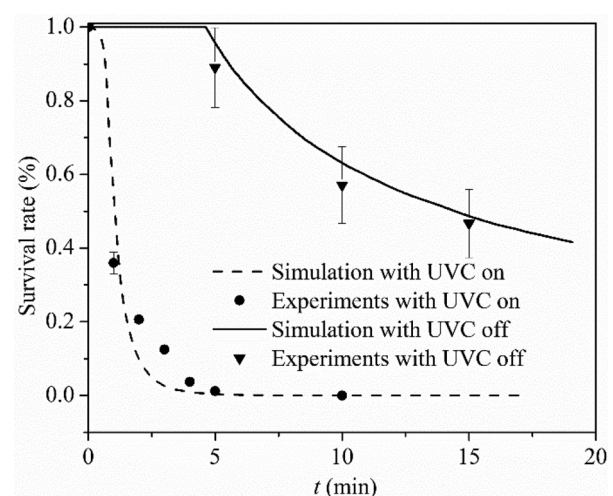**FIG. 6.** (a) BSC chamber with UVC prototype and (b) schematic diagram for the UVC prototype.

FIG. 7. Comparisons between experimental and simulation results for BSC chamber.

numerical model. With the numerical model validated, it will be applied for the simulation of air disinfection in air duct.

IV. RESULTS AND DISCUSSION

A. LED module performance in air duct

The input electrical power and UVC irradiation output power for each LED chip are 0.42 W and 7 mW, respectively. The operation temperature of the LED module is critical for disinfection performance as well as the LED lifespan. In order to monitor the LED module temperature, four thermocouples are mounted on the LED panels. Figure 8 shows the top view for the locations of four thermocouple sensors. The outputs of the thermocouple sensors are recorded via a multi-channel reader. As shown in Fig. 8, LED panel A on the left is single-sided, which means that one side of the heat pipe is attached with two LED strips shining toward right. It is the same for the LED panel B on the right side. However, the central LED panel C is double-sided where both sides of the heat pipe are attached with two LED strips.

Figures 9(a) and 9(b) show temperature variations at the four locations without and with air flow in the air duct when the LED module operates, respectively. Two different tests with fan off and on are studied, representing the case without air flow and with air flow in the air duct, respectively. When the fan is off in the first test, it is obvious that the temperature from all the locations increases with time, as seen from Fig. 9(a). This indicates the insufficient heat dissipation through natural convection between air and heat sinks. We turned off the LEDs after 10 min when the temperature for CH2 and CH4 sensors are over 50 °C to avoid the overheat of LED modules. The safe operation temperature of the LED chip is 60 °C according to the LED specification.

In the second test with fan on, air with a flow rate of 9000 l/min is pumped into the air duct with temperature of 23 °C. The variation of temperature at the four locations is shown in Fig. 9(b). Generally, temperature increases initially and approaches to constant value after 20 min for all the locations. The temperature for CH2 and CH4 sensors are close to each other and they are higher than that of CH1 and
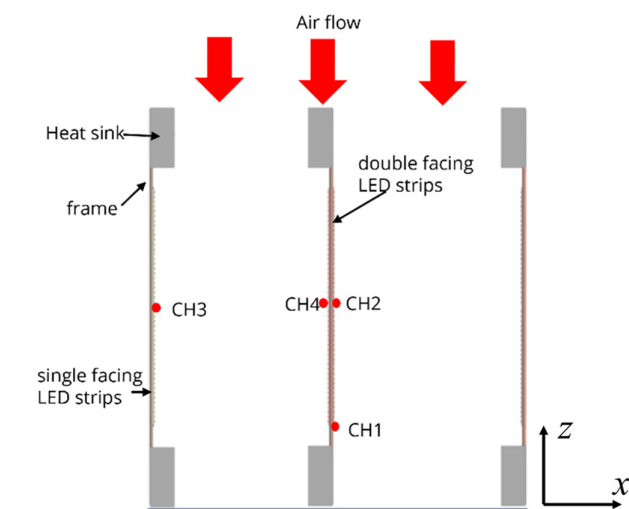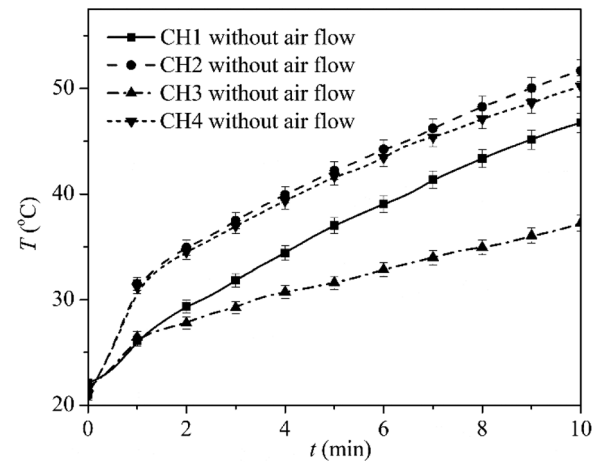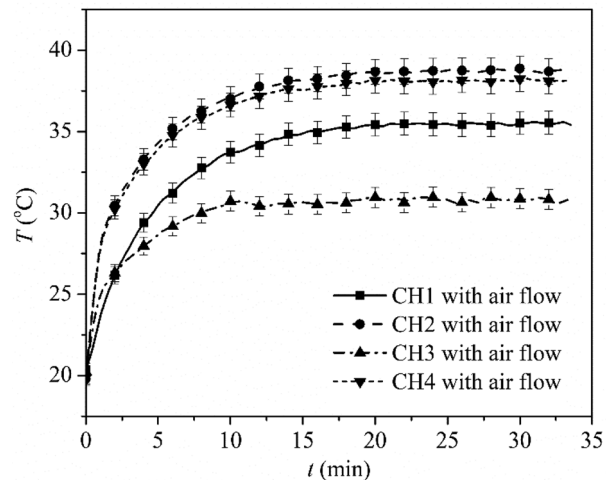

(a)

(b)

FIG. 9. Reliability test for the temperature distribution along the LED module with (a) fan off and (b) fan on at flow rate of 9000 l/min.

CH3. The middle LED panel C has twice as many as LEDs compared with the LED panels A and B near the duct walls, leading to a much higher heat dissipation. Therefore, the temperature in the middle LED panel C is higher than that near the duct walls. CH1 is located near the tip of the LED panel C where the fins are attached. Convection heat transfer is significantly increased with the large exposed surface area between the fins and air, resulting in a low temperature at CH1 compared to CH2 and CH4. It is clear that the temperature for all the tested locations is well below 40 °C which is safely below the maximum operation tempeautre of 60 °C for LEDs. This demonstrates the heat removal capability of the heat sink design. It is calculated that air temperature out of the duct is around 24.4 °C based on the flow rate of 9000 l/min. Given the small temperature change in the duct, the heat effect of the UVC LED and heat panels on the air flow can be neglected.

FIG. 8. Top view of thermocouple locations for the LED module.

## B. Air disinfection performance in a meeting room

With the stability test to ensure UVC LED module working under the safe operation temperature, air disinfection performance for the LED module is tested when air duct is placed in a meeting room, as shown in Figs. 10(a)–10(c). The dimensions of the meeting room are 9.2 m in length, 3.9 m in width, and 3.0 m in height, with a total volume of 107 m^3. The schematic diagram for the top view of the room is shown in Fig. 10(a). The air flow rate in the duct is adjusted to 9000 l/min which leads to around 12 min for an air exchange, i.e., an equivalent to five air change per hour (ACH) of the whole room.

The test was conducted during the COVID pandemic lockdown period with majority of staffs working from home. The actual baseline of bacteria numbers in the meeting room is measured every 2 min with a total duration of 12 min. To raise the baseline to a reasonable level for testing, and to further mimic the situation of post pandemic when people talk or drink in the meeting room, 15 cups of coconut milk with each of 50 ml are randomly placed on the table of the room at different locations for 50 h. The meeting room is closed and none of the ventilation solutions are used. The average room temperature is around 30 °C which makes the coconut milk spoiled within one day.

The contaminated milk with bacterial evaporates into air, resulting in the increase of the bacterial numbers in the room. The coconut milk is chosen here as it generates less harmful microbes compared with other bacteria. Although there might be different types of bacteria in the room, the susceptibility of one bacterium could be different from another. However, comparisons will be made for the survival ratio for all the bacteria before and after UVC LED operates.

Three air samplers, i.e., A, B, and C, are placed at different locations of the room. The air sampling duration and volume are 2 min and 200 ml, respectively. Air samplers and agar plates are used to count numbers of bacteria in the air. The agar plate is placed inside the chamber of an air sampler. Bacteria flowing through the air sampler will hit and then be trapped onto the surface of the agar plate. The agar plates are then placed into an oven with a constant temperature for 48 h for bacteria to grow and be counted.
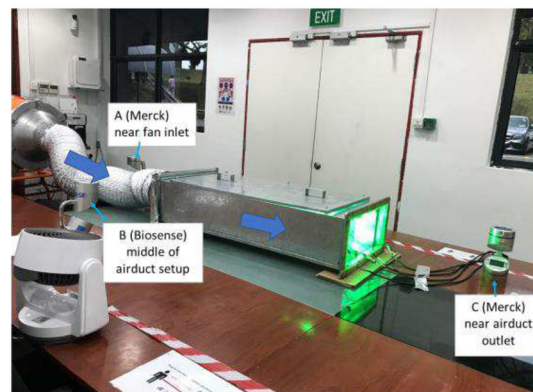
Since there might be different types of bacteria in the meeting room when coconut milk spoiled, the inactivation rate constant is, thus, unknown. Therefore, simulation is only performed for UVI distribution in the air duct. The contour plots for the UVI radiation fields at three selected cutting planes, i.e., $y = 15$, 60, and 115 mm starting
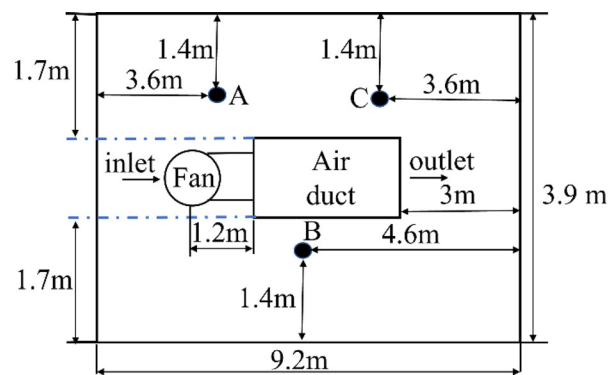

(a)
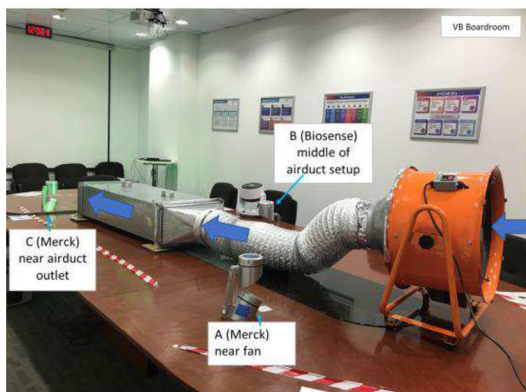
(b)

(c)

FIG. 10. (a) Schematic diagram for the top view of the room and the locations for air duct as well as air samplers (not to scale), (b) picture for duct section with the LED module, and (c) operation of the LED module.

17 August 2024 08:19:13

from the bottom of the channel, are shown in Fig. 11(a). Generally, the further the location away from the LED chips, the smaller the UVI values. Figure 11(b) shows the flow path lines in the module colored by the flow velocity. Recirculation is observed near the inlet corner of the duct.

Six UV sensors are arranged at different locations of the air duct. Comparisons between experiments and simulation for the UVI values along the centerline of the middle LED strip on the left-hand side of the air duct is shown in Fig. 12. x is the distance from the LED strip near the left wall. It is noted that the UVI value decreases significantly when the distance from the LED strip increases. It starts to increase as approaches to the middle LED strip. Generally, reasonable agreement is achieved between experiments and simulation results.
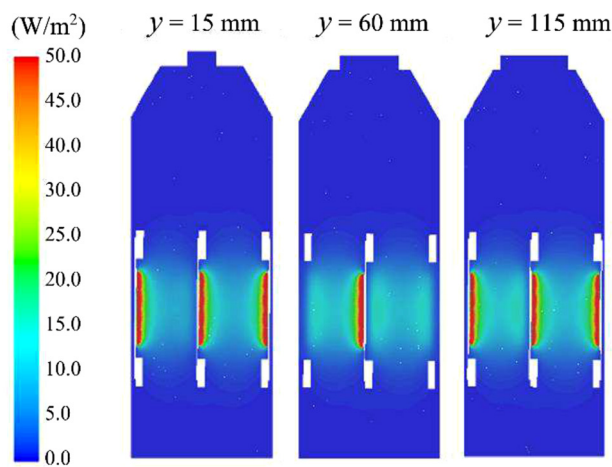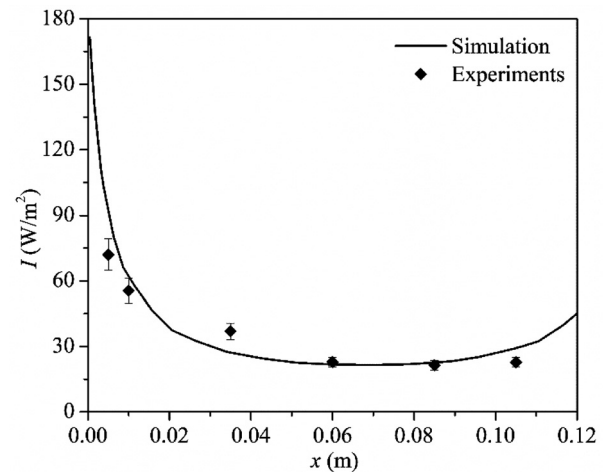

(a)
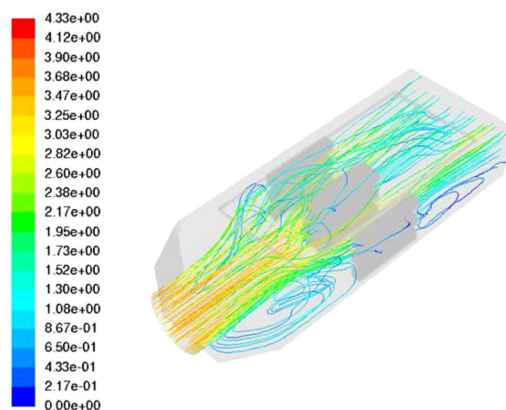
(b)

FIG. 11. (a) Radiation profile at $y = 15$, 60, and 115 mm starting from the bottom of the channel and (b) the flow path lines colored by velocity under the flow rate of 9000 l/min and LED power of 7 mW.


FIG. 12. UVI comparison between experiments and simulation under flow rate of 9000 l/min and LED power of 7 mW.

Figure 13(a) demonstrates the disinfection effect of the LED module in terms of pathogen survival ratio vs disinfection time. Experiments are performed without coconut milk in the rooms as a baseline. The pathogen number at three locations, i.e., A, B, and C, is sampled every 2 min with a total duration of 90 min. The pathogen number for the baseline is around 110, 190, and 70 CFU/m^3 at A, B, and C, respectively. With coconut milk spoiled in the room for 50 h, the initial counts of pathogen number in the three sample locations increased to 1300, 780, and 700 CFU/m^3 at A, B, and C, respectively. It is seen from Fig. 13(a) that the pathogen number for all the measuring locations reduces significantly once the air duct system starts to work. For example, the pathogen counts dropped from 1300 to 350 CFU/m^3 at location A, indication of more than 73% reduction of the pathogen within 60 min. Further reduction in the pathogen counts is observed when air duct system works for another 30 min. Similar trends can be seen for locations B and C. The dimensionless survival ratio under different times is plotted in Fig. 13(b). The dimensionless survival ratio is calculated by dividing the pathogen counts by the averaged pathogen counts at the three samplers for the baseline. It is clear to see from both Figs. 13(a) and 13(b) that the number of the pathogen counts in the meeting room increases significantly when coconut milk spoiled. With UVC LED operates, such high number of the pathogen reduces gradually, an indication of the effectiveness for UVC LED in killing or inactivation of the pathogen. It is also noted that the dimensionless survival ratios for the three locations are all larger than one at $t = 90$ min. This suggests that the UVC LED is unable to kill or inactivate all the pathogen generated by the coconut milk. There is a possibility that a small portion of the generated bacteria has higher UV resistance. Nevertheless, it is found that more than 85% of the pathogen has been disinfected by UVC LED modules within 90 min.
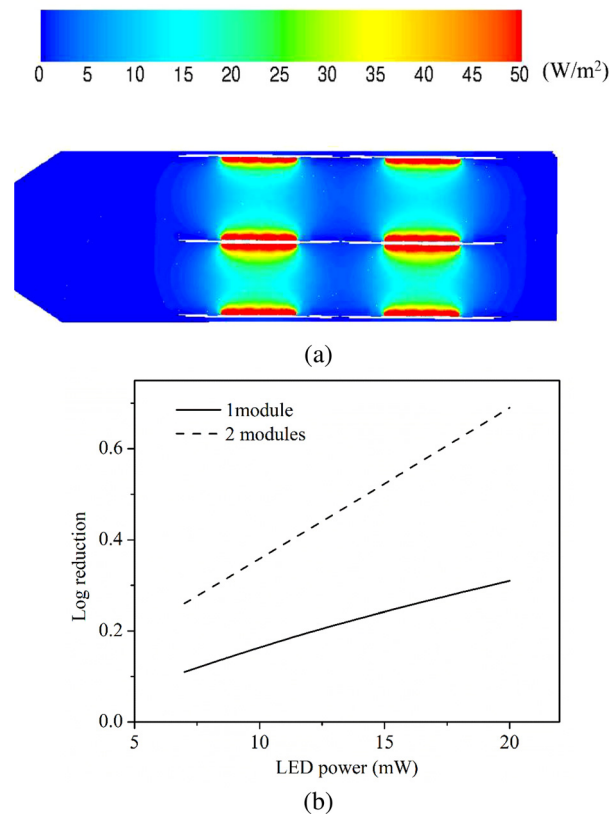
C. Effect of multiple UVC LED modules in air duct

The current LED module is easy to install and scale up in the air duct. It can be adopted in various air ducts with different sizes and air flow rates. We have simulated two LED modules in series in an air duct. The comparisons are made between a single LED module and

17 August 2024 08:19:13
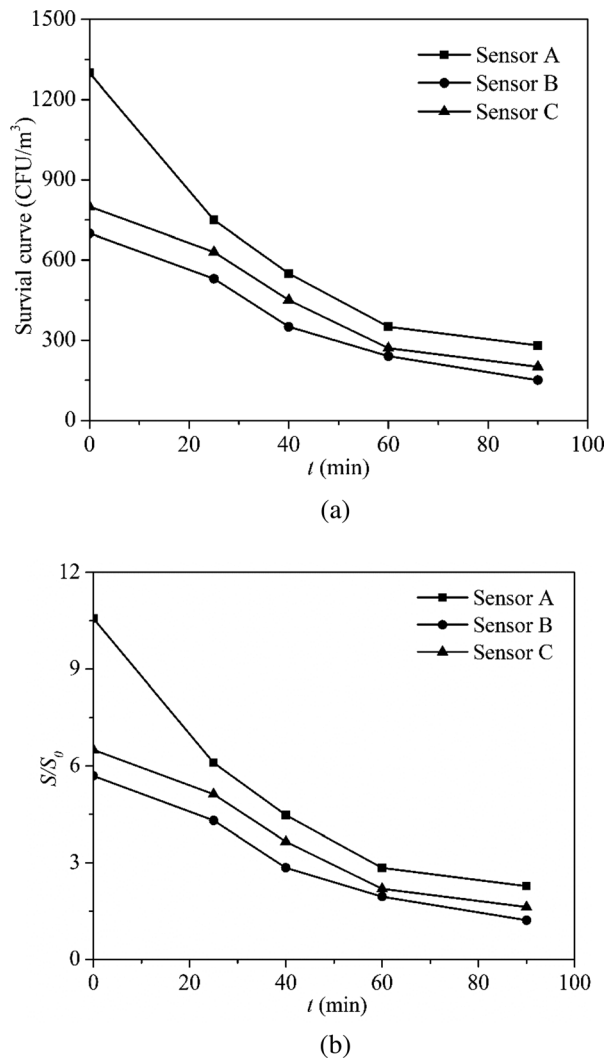
FIG. 13. Variation of (a) survival pathogen and (b) dimensionless survival ratios under different times.

FIG. 14. (a) UVI distribution for two UVC LED modules along the flow direction and (b) comparisons of log reduction between one and two UVC LED modules.

two LED modules for air disinfection under different LED powers. *E. coli* is used as the bacteria with the inactivation constant of 0.44 cm^2/mJ.[40] The diameter of *E. coli* is chosen to be 30 μm. Figure 14 (a) shows the UVI distribution at the center cutting plane along the flow direction. With the second UVC LED module arranged after the first module, the pathogen can continue absorbing UV dose when it passes by. This will increase the inactivation rate. The effect of LED power on the log reduction for both one and two UVC LED modules is shown in Fig. 14(b). Log reduction is calculated based on the procedure used in Li *et al.*[39] Note that the results are only obtained from a single path of the pathogen across the air duct. As expected, log reduction increases with the increase of the LED power. It is also observed that the two LED module can achieve more than two times of log reduction compared with that of one module. The log reduction is as high as 0.7 for a single path based on the current two-module design

under LED power of 20 mW, leading to 80% disinfection rate for the air duct system. Given the advancement of LED technology in recent years, the radiation power of UVC LED is expected to increase significantly.[21] This will bring the great potential for UVC LED to disinfect air in HVAC system.

Experimental study related to the inactivation of the SARS-CoV-2 virus by using the current UVC LED module is a challenge due to the constrained testing environment. Such experimental test will be one of our future work. Nevertheless, we have compared the simulation results based on the two UVC LED module system with the existing available data.[41,42] Luo and Zhong[41] have predicted that UV dose above 4.47 J/m^2 could achieve log reduction of 0.96, i.e., equivalent to 89.10%, for SARS-CoV-2 virus inactivation. A higher UV dose of 11.17 J/m^2 results in a two-log reduction which indicates that 99% of SARS-CoV-2 virus is inactivated.[41] Similar results are reported by Buonanno *et al.*[42] With reference to these values, we have analyzed the UV dose absorbed by each individual pathogen from our simulation results. Figure 15 plots the histogram of UV dose under 7 mW with two UVC LED modules in the air duct when ACH is five. It allows us to see how many pathogens receive adequate UV dose to be inactivated when SARS-CoV-2 virus is considered. It is clear that more than 99.70% pathogen receives UV dose larger than 4.47 J/m^2 within one hour, resulting in an almost 89.10% disinfection rate by using the two
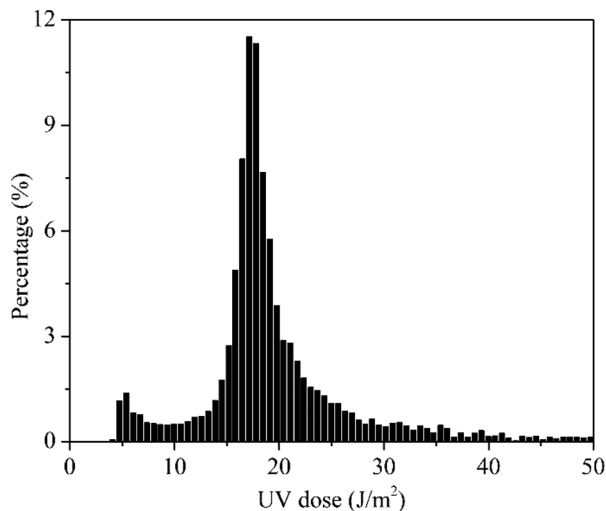
FIG. 15. Histogram of UV dose for two UVC LED modules under flow rate of 9000 l/min and LED power of 7 mW.

UVC LED modules. Further verification on UV dose shows that around 80.89% of pathogen receives UV dose higher than 11.17 J/m². This demonstrates the capability of the current UVC LED modules to be used for the mitigation of SARS-CoV-2 airborne transmission in buildings. However, it is necessary to mention that the viability of the SARS-CoV-2 virus in air is highly dependent on temperature and humidity. This is beyond the scope of the current work. The results provided here only give some reference for the efficacy of the developed UVC LED module in this work. Detailed experiments for disinfection of SARS-CoV-2 virus by using the UVC LED module will be carried out as one of our future works.

V. CONCLUSIONS

We have developed UVC LED modules in air duct to evaluate its disinfection performance. The UVC LED module proposed is flexible to install in air ducts with varied sizes for different flow rates. The module is easy to scale up to achieve a high disinfection rate. Both experiments and simulations are carried out to study the inactivation rate of the system. It is demonstrated that the current one UVC LED module can achieve more than 70% disinfection rate within 60 min in a meeting room with 107 m³ under LED power of 7 mW. The disinfection rate is more than two times for the two-module system compared with one module system. Such disinfection performance is expected to increase further with the increase of LED power. The prediction for the disinfection rate based on SARS-CoV-2 virus shows that the two-module system is able to disinfect more than 80% of the virus within 60 min in the same meeting room. The current work shows that UVC LED is an extremely promising candidate for air duct disinfection in the HVAC system.

ACKNOWLEDGMENTS

AUTHOR DECLARATIONS
Conflict of Interest

The authors have no conflicts to disclose.

Author Contributions

Hongying Li: Conceptualization (equal); Formal analysis (equal); Methodology (equal); Project administration (equal); Supervision (equal); Validation (equal); Writing – original draft (equal); Writing – review & editing (equal). **Xuechuan Shan:** Conceptualization (equal); Data curation (equal); Writing – original draft (equal). **Te Ba:** Methodology (equal); Writing – original draft (equal). **Yu Chan Liu:** Data curation (equal); Methodology (equal); Validation (equal). **Chang-Wei Kang:** Data curation (equal); Methodology (equal); Validation (equal). **Candice Au Ka Hing:** Data curation (equal); Formal analysis (equal). **Nitin Loganathan:** Data curation (equal); Validation (equal). **Uvarajan M. Velayutham:** Data curation (equal); Methodology (equal).

DATA AVAILABILITY

The data that support the findings of this study are available from the corresponding author upon reasonable request.

REFERENCES

[1]See https://covid19.who.int/ for "WHO website;" accessed 13 March 2023.
[2]R. Mittal, R. Ni, and J. H. Seo, "The flow physics of COVID-19," J. Fluid Mech. **894**, F2-1–F2-14 (2020).
[3]Y. Shen, C. W. Li, H. J. Dong, Z. Wang, L. Martinez, Z. Sun *et al.*, "Community outbreak investigation of SARS-CoV-2 transmission among bus riders in eastern China," JAMA Intern. Med. **180**, 1665–1671 (2020).
[4]J. Lu, J. N. Gu, K. B. Li, C. H. Xu, W. Z. Su, Z. S. Lai, D. Q. Zhou, C. Yu, B. Xu, and Z. C. Yang, "COVID-19 outbreak associated with air conditioning in restaurant, Guangzhou, China, 2020," Emerging Infect. Dis. **26**, 1628–1631 (2020).
[5]P. Katre, S. Banerjee, S. Balusamy, and K. C. Sahu, "Fluid dynamics of respiratory droplets in the context of COVID-19: Airborne and surfaceborne transmissions," Phys. Fluids **33**, 081302 (2021).
[6]S. Y. Park, Y. Kim, S. Yi, S. Lee, B. Na, C. B. Kim *et al.*, "Coronavirus disease outbreak in call center South Korea," Emerging Infect. Dis. **26**, 1666–1670 (2020).
[7]S. Asadi, N. Bouvier, A. S. Wexler, and W. D. Ristenpart, "The coronavirus pandemic and aerosols: Does COVID-19 transmit via expiratory particles?," Aerosol Sci. Technol. **54**, 635–638 (2020).
[8]S. Burgmann and U. Janoske, "Transmission and reduction of aerosols in classrooms using air purifier systems," Phys. Fluids **33**, 033321 (2021).
[9]M. Raeiszadeh and B. Adeli, "A critical review on ultraviolet disinfection systems against COVID-19 outbreak: Applicability, validation, and safety considerations," ACS Photonics **7**, 2941–2951 (2020).
[10]A. Suwardi, C. C. Ooi, D. Daniel, C. K. I. Tan, H. Y. Li, Z. L. Ou Yang *et al.*, "The efficacy of plant-based ionizers in removing aerosol for COVID-19 mitigation," Research **2021**, 2173642.
[11]See the section on enhancing air filtration and cleaning at https://www.epa.gov/indoor-air-quality-iaq/clean-air-buildings-challenge for information about UVGI systems; accessed 13 March 2023.
[12]N. G. Reed, "The history of ultraviolet germicidal irradiation for air disinfection," Public Health Rep. **125**, 15–27 (2010).
[13]V. D'Alessandroa, M. Falone, L. Giammichele, and R. Ricci, "Eulerian–Lagrangian modeling of cough droplets irradiated by ultraviolet–C light in relation to SARS-CoV-2 transmission," Phys. Fluids **33**, 031905 (2021).

[14]M. Biasin, A. Bianco, G. Pareschi, A. Cavalleri, C. Cavatorta, C. Fenizia *et al.*, "UV-C irradiation is highly effective in inactivating SARS-CoV-2 replication," Sci. Rep. **11**, 6260 (2021).

[15]N. Trivellin, M. Buffolo, F. Onelia, A. Pizzolato, M. Barbato, V. T. Orlandi *et al.*, "Inactivating SARS-CoV-2 using 275 nm UV-C LEDs through a spherical irradiation box: Design, characterization and validation," Materials **14**, 2315 (2021).

[16]M. Bormann, M. Alt, L. Schipper, L. van de Sand, M. Otte, T. L. Meister, U. Dittmer, O. Witzke, E. Steinmann, and A. Krawczyk, "Disinfection of SARS-CoV-2 contaminated surfaces of personal items with UVC-LED disinfection boxes," Viruses **13**, 598 (2021).

[17]Z. B. Feng, S. J. Cao, and F. Haghighat, "Removal of SARS-CoV-2 using UV+ filter in built environment," Sustainable Cities Soc. **74**, 1032236 (2021).

[18]L. Sehulster and R. Y. Chinn, "Guidelines for environmental infection control in health-care facilities. Recommendations of CDC and the Healthcare Infection Control Practices Advisory Committee (HICPAC)," MMWR Recomm Rep. **52**, 1–42 (2003).

[19]T. Ethington, S. Newsome, J. Waugh, and L. D. Lee, "Cleaning the air with ultraviolet germicidal irradiation lessened contact infections in a long-term acute hospital," Am. J. Infect. Control **46**, 482–486 (2018).

[20]B. Lee and W. P. Bahnfleth, "Effects of installation location on performance and economics of in-duct ultraviolet germicidal irradiation systems for air disinfection," Build. Environ. **67**, 193–291 (2013).

[21]N. Trivellin, D. Fiorimonte, F. Piva, M. Buffolo, C. D. Santi, G. Meneghesso, E. Zanoni, and M. Meneghini, "Reliability of Commercial UVC LEDs: 2022 state-of-the-art," Electronics **11**, 728 (2022).

[22]D. K. Kim and D. H. Kang, "UVC LED irradiation effectively inactivates aerosolized viruses, bacteria, and fungi in a chamber-type air disinfection system," Appl. Environ. Microbiol. **84**, e00944–18 (2018).

[23]T. Mathebula, F. W. Leuschner, and S. Chowdhury, "The use of UVC-LEDs for the disinfection of Mycobacterium Tuberculosis," in *IEEE PES/IAS Power Africa* (IEEE, 2018), pp. 739–744.

[24]S. S. Nunayon, H. H. Zhang, and A. C. K. Lai, "A novel upper-room UVC-LED irradiation system for disinfection of indoor bioaerosols under different operating and airflow conditions," J. Hazard. Mater. **396**, 122715 (2020).

[25]A. C. K. Lai and S. S. Nunayon, "A new UVC-LED system for disinfection of pathogens generated by toilet flushing," Indoor Air **31**, 324–334 (2021).

[26]S. S. Nunayon, H. H. Zhang, V. Chan, R. Y. C. Kong, and A. C. K. Lai, "Study of synergistic disinfection by UVC and positive/negative air ions for aerosolized *Escherichia coli*, *Salmonella typhimurium*, and *Staphylococcus epidermidis* in ventilation duct flow," Indoor Air **32**, e12957 (2021).

[27]ANSYS, *ANSYS–FLUENT 12.0 Theory Guide* (ANSYS, 2012).

[28]A. B. Halima, Z. Araoud, L. Canale, K. Charrada, and G. Zissis, "Energy efficiency of a LED lighting system using a Peltier module thermal converter," Case Stud. Therm. Eng. **34**, 101989 (2022).

[29]W. P. Jones and B. E. Launder, "The prediction of laminarization with a two-equation model of turbulence," Int. J. Heat Mass Transfer **15**, 301–314 (1972).

[30]Q. Xu, J. X. Feng, J. Z. Zhou, L. Liu, Y. Zang, and H. B. Fan, "Study of a new type of radiant tube based on the traditional M-type structure," Appl. Therm. Eng. **150**, 849–857 (2019).

[31]D. A. Sozzi and F. Taghipour, "Computational and experimental study of annular photo-reactor hydrodynamics," Int. J. Heat Fluid Flow **27**, 1043–1053 (2006).

[32]S. Elyasi and F. Taghipour, "Simulation of UV photoreactor for water disinfection in Eulerian framework," Chem. Eng. Sci. **61**, 4741–4749 (2006).

[33]B. E. Launder and D. B. Spalding, *Lectures in Mathematical Models of Turbulence* (Academic Press, London, 1972).

[34]H. K. Versteeg and W. Malalasekera, *An Introduction to Computational Fluid Dynamics, the Finite Volume Method*, 2nd ed. (Pearson Education Limited, 2007).

[35]G. D. Raithby and E. H. Chui, "A finite-volume method for predicting a radiant heat transfer in enclosures with participating media," J. Heat Transfer **112**, 415–423 (1990).

[36]P. A. Cundall and O. D. L. Strack, "A discrete numerical model for granular assemblies," Géotechnique **29**, 47–65 (1979).

[37]S. A. Moris and A. J. Alexander, "An investigation of particle trajectories in two-phase flow systems," J. Fluid Mech. **55**, 193–208 (1972).

[38]H. Y. Li, H. Osman, C. W. Kang, and T. Ba, "Numerical and experimental investigation of UV disinfection for water treatment," Appl. Therm. Eng. **111**, 280–291 (2017).

[39]H. Y. Li, H. Osman, C. W. Kang, and T. Ba, "Numerical and experimental study for water treatment by using UV reactors," Water Sci. Technol. **80**, 1456–1465 (2019).

[40]N. Loganathan, S. Kannan, M. Z. R. Tay, Y. L. Huang, J. Tan, U. Velayutham, Y. Y. Ooi, W. T. Ang, F. Yu, C. W. Kang, T. Ba, H. Y. Li, Y. Y. Yang, and M. N. Win, "Germicidal effect of 275 nm UVC LEDs against airborne microorganisms accessed in a benchtop testing setup," Environ. Microbiol. (submitted).

[41]H. Luo and L. X. Zhong, "Ultraviolet germicidal irradiation (UVGI) for in-duct airborne bioaerosol disinfection: Review and analysis of design factors," Build. Environ. **197**, 107852 (2021).

[42]M. Buonanno, D. Welch, I. Shuryak, and D. J. Brenner, "Far-UVC light (222 nm) efficiently and safely inactivates airborne human coronaviruses," Sci. Rep. **10**, 1–8 (2020).

17 August 2024 08:19:13